Metal-insulator transition in three-band Hubbard model with strong spin-orbit interaction

Liang Du and Xi Dai
Beijing National Laboratory for Condensed Matter Physics,
and Institute of Physics, Chinese Academy of Sciences, Beijing 100190, China

Li Huang
Beijing National Laboratory for Condensed Matter Physics, and Institute of Physics,
Chinese Academy of Sciences, Beijing 100190, China   and
Science and Technology on Surface Physics and Chemistry Laboratory,
P.O. Box 718-35, Mianyang 621907, Sichuan, China
(Dated: November 12, 2012)

Recent investigations suggest that both spin-orbit coupling and electron correlation play very crucial roles in the $5d$ transition metal oxides. By using the generalized Gutzwiller variational method and dynamical mean-field theory with the hybridization expansion continuous time quantum Monte Carlo as impurity solver, the three-band Hubbard model with full Hund's rule coupling and spin-orbit interaction terms, which contains the essential physics of partially filled t_{2g} sub-shell of $5d$ materials, is studied systematically. The calculated phase diagram of this model exhibits three distinct phase regions, including metal, band insulator and Mott insulator respectively. We find that the spin-orbit coupling term intends to greatly enhance the tendency of the Mott insulator phase. Furthermore, the influence of the electron-electron interaction on the effective strength of spin-orbit coupling in the metallic phase is studied in detail. We conclude that the electron correlation effect on the effective spin-orbit coupling is far beyond the mean-field treatment even in the intermediate coupling region.

I. INTRODUCTION

The Mott metal-insulator transition (MIT) induced by electron-electron correlation has attracted intensive research activities in the past several decades[1–4]. Although the main features of Mott transition have already been captured by single-band Hubbard model, most of Mott transition in realistic materials have multi-orbital nature and should be described by multi-band Hubbard model. Unlike the situation in single-band case, where the Mott transition is completely driven by the local Coulomb interaction U, the Mott transition in multi-band case is affected by not only Coulomb interaction but also crystal field splitting and Hund's rule coupling among different orbitals[5–7]. The interplay between Hund's rule coupling and crystal field splitting generates lots of interesting phenomena in the multi-band Hubbard model, for examples, orbital selective Mott transition, high-spin to low-spin transition and orbital ordering. Therefore, most of the intriguing physics in $3d$ or $4d$ transition metal compounds can be well described by the multi-band Hubbard model with both Hund's rule coupling and crystal field splitting.

In the present paper, we would like to concentrate our attention on the Mott physics in another group of interesting compounds, the $5d$ transition metal compounds, where spin-orbit coupling (SOC), the new physical ingredient in Mott physics, plays an important role. Compared to $3d$ orbitals, the $5d$ orbitals are much more extended and the correlation effects are not expected to be important here. While as firstly indicated in reference[8], the correlation effects can be greatly enhanced by SOC,

which is commonly strong in $5d$ materials. The first well studied $5d$ Mott insulator with strong SOC is Sr_2IrO_4, where the SOC splits the t_{2g} bands into (upper) $j_{\text{eff}} = 1/2$ doublet and (lower) $j_{\text{eff}} = 3/2$ quartet bands and greatly suppresses their bandwidths[8–12]. Since there are totally five electrons in its $5d$ orbitals, the $j_{\text{eff}} = 1/2$ bands are half filled and the $j_{\text{eff}} = 3/2$ bands are fully occupied, which makes the system being effectively a $j_{\text{eff}} = 1/2$ single-band Hubbard model with reduced bandwidth. Therefore the checkerboard anti-ferromagnetic ground state of Sr_2IrO_4 can be well described by the single-band Hubbard model with half filling.

Here, we will focus on the $5d$ materials with four electrons in the t_{2g} sub-shell. These materials include the newly discovered $BaOsO_3$, $CaOsO_3$ and $NaIrO_3$ etc[13]. All these materials share one important common feature: in low temperature, these materials are insulators without magnetic long-range order. The origin of the insulator behavior can be due to two possible reasons, the strong enough Coulomb interaction and SOC. We will have Mott insulator in the former and band insulator in the latter case respectively. Therefore it is interesting to study the features of metal-insulator transition in a generic t_{2g} system occupied by four electrons with both Coulomb interaction and SOC.

In the present paper, we study the t_{2g} Hubbard model with SOC and four electrons filling by using rotational invariant Gutzwiller approximation (RIGA) and dynamical mean-field theory combined with the hybridization expansion continuous time quantum Monte Carlo (DMFT + CTQMC) respectively. The paramagnetic $U - \zeta$ phase diagram is derived carefully. Further, the interplay be-

tween SOC ζ and Coulomb interaction U is analyzed in detail. We will mainly focus on the following two key issues: (i) How does the SOC affect the boundary of Mott transitions in this three-band model? (ii) How does the Coulomb interaction modify the effective SOC strength?

This paper is organized as follows. In Sec. II, the three-band model is specified, and the generalized multi-band Gutzwiller variational wave function is introduced. In Sec. III A, the calculated results, including $U - \zeta$ phase diagram, quasi-particle weight and charge distribution, for the three-band model are presented. The effect of Coulomb interaction on SOC is analyzed in Sec. III B. Finally we make conclusions in section IV.

II. MODEL AND METHOD

The three-band Hubbard model with full Hund's rule coupling and SOC terms is defined by the Hamiltonian:

$$H = -\sum_{ij,a\sigma} t_{ij} d^{\dagger}_{i,a\sigma} d_{j,a\sigma} + \sum_i H^i_{loc} = H_{kin} + H_{loc}, \quad (1)$$

where σ denotes electronic spin, and a represents the three t_{2g} orbitals with $a = 1, 2, 3$ corresponding to d_{yz}, d_{zx}, d_{xy} orbitals respectively. The first term describes the hopping process of electrons between spin-orbital state "$a\sigma$" on different lattice sites i and j. Local Hamiltonian terms $H^i_{loc} = H^i_u + H^i_{soc}$ contain Coulomb interaction H^i_u and SOC H^i_{soc} (In the following, the site index is suppressed for sake of simplicity).

$$H_u = U \sum_a n_{a\uparrow} n_{a\downarrow} + U' \sum_{a<b,\sigma\sigma'} n_{a\sigma} n_{b\sigma'} - J_z \sum_{a<b,\sigma} n_{a\sigma} n_{b\sigma}$$
$$- J_{xy} \sum_{a<b} \left(d^{\dagger}_{a\uparrow} d_{a\downarrow} d^{\dagger}_{b\downarrow} d_{b\uparrow} + d^{\dagger}_{a\uparrow} d^{\dagger}_{a\downarrow} d_{b\uparrow} d_{b\downarrow} + h.c. \right), (2)$$

$$H_{soc} = \sum_{a\sigma} \sum_{b\sigma'} \zeta \langle a\sigma | l_x s_x + l_y s_y + l_z s_z | b\sigma' \rangle d^{\dagger}_{a\sigma} d_{b\sigma'}, \quad (3)$$

where U (U') denotes the intra-orbital (inter-orbital) Coulomb interaction, J_z term describes the longitudinal part of the Hund's coupling. While the other two J_{xy} terms describe the spin-flip and pair-hopping process respectively. ζ is SOC strength, $l(s)$ is orbital (spin) angular momentum operator. Here we assume the studied system experiences approximately cubic symmetry (O_h symmetry), in which two parameters U' and J_{xy} follow the constraints $U' = U - 2J$ and $J_{xy} = J_z = J$. Here we choose $J/U = 0.25$ for the systems studied in this paper unless otherwise noted. This lattice model is solved in the framework of RIGA[14–17] and DMFT(CTQMC)[18,19] methods respectively, which are both exact in the limit of infinite spacial dimensions[20,21]. In this work, a semi-elliptic bare density of states $\rho(\epsilon) = (2/\pi D)\sqrt{1 - (\epsilon/D)^2}$ is adopted, which corresponds to Bethe lattice with infinite connectivity. In the present study, the energy unit

is set to be half bandwidth $D = 1$ and all orbitals are assumed to have equal bandwidth.

Next, we will briefly introduce the recently developed RIGA method[16]. The generalized Gutzwiller trial wave function $|\Psi_G\rangle$ can be constructed by acting a many-particle projection operator $\mathcal{P}$ on the uncorrelated wave function $|\Psi_0\rangle$[22–24],

$$|\Psi_G\rangle = \mathcal{P}|\Psi_0\rangle, \quad (4)$$

with

$$\mathcal{P} = \prod_i \mathcal{P}_i = \prod_i \sum_{\Gamma\Gamma'} \lambda_{\Gamma\Gamma'} |\Gamma\rangle_{ii} \langle \Gamma'|. \quad (5)$$

$|\Psi_0\rangle$ is normalized uncorrelated wave function in which Wick's theorem holds. $|\Gamma\rangle_i$ are atomic eigenstates on site i and $\lambda_{\Gamma\Gamma'}$ are Gutzwiller variational parameters. In our work, $|\Gamma\rangle_i$ are eigenstates of atomic Hamiltonian H_u, each $|\Gamma\rangle_i$ is labeled by good quantum number $\mathcal{N}, \mathcal{J}, \mathcal{J}_z$, where $\mathcal{N}$ is total number of electrons, $\mathcal{J}$ is total angular momentum, $\mathcal{J}_z$ is projection of total angular momentum along z direction. The non-diagonal elements of the previously defined variational parameter matrix $\lambda_{\Gamma\Gamma'}$ are assumed to be finite only for state $|\Gamma\rangle$, $|\Gamma'\rangle$ belonging to the same atomic multiplet, i.e, with the same three quantum labels[15]. In the following, we assume the local Fock terms are absent in $|\Psi_0\rangle$,

$$\langle \Psi_0 | c^{\dagger}_{i\alpha} c_{i\beta} | \Psi_0 \rangle = \delta_{\alpha\beta} \langle \Psi_0 | c^{\dagger}_{i\alpha} c_{i\alpha} | \Psi_0 \rangle = \delta_{\alpha\beta} n^0_{i\alpha}. \quad (6)$$

For general case, a local unitary transformation matrix $\mathcal{A}$ is needed to transform the original $d_{i\alpha}$-basis into the so-called natural c_{im}-basis[16], i.e, $d_\alpha = \sum_m \mathcal{A}_{\alpha m} c_m$. In the original single particle basis ($d_{yz}\uparrow, d_{yz}\downarrow, d_{zx}\uparrow, d_{zx}\downarrow, d_{xy}\uparrow, d_{xy}\downarrow$), SOC term is expressed as :

$$H_{soc} = -\frac{\zeta}{2} \begin{pmatrix} 0 & 0 & -i & 0 & 0 & 1 \\ 0 & 0 & 0 & i & -1 & 0 \\ i & 0 & 0 & 0 & 0 & -i \\ 0 & -i & 0 & 0 & -i & 0 \\ 0 & -1 & 0 & i & 0 & 0 \\ 1 & 0 & i & 0 & 0 & 0 \end{pmatrix}. \quad (7)$$

Then the transformation matrix $\mathcal{A}$ is as follows:

$$\mathcal{A} = \frac{1}{\sqrt{6}} \begin{pmatrix} -\sqrt{3} & 0 & 1 & 0 & 0 & -\sqrt{2} \\ 0 & -1 & 0 & \sqrt{3} & -\sqrt{2} & 0 \\ -i\sqrt{3} & 0 & -i & 0 & 0 & i\sqrt{2} \\ 0 & -i & 0 & -i\sqrt{3} & -i\sqrt{2} & 0 \\ 0 & 2 & 0 & 0 & -\sqrt{2} & 0 \\ 0 & 0 & 2 & 0 & 0 & \sqrt{2} \end{pmatrix}, \quad (8)$$

where the t_{2g} orbitals have been treated as a system with $l_{\text{eff}} = 1$.

In the natural single particle basis, SOC matrix is transformed into:

$$H_{soc} = \begin{pmatrix} -\zeta/2 & 0 & 0 & 0 & 0 & 0 \\ 0 & -\zeta/2 & 0 & 0 & 0 & 0 \\ 0 & 0 & -\zeta/2 & 0 & 0 & 0 \\ 0 & 0 & 0 & -\zeta/2 & 0 & 0 \\ 0 & 0 & 0 & 0 & \zeta & 0 \\ 0 & 0 & 0 & 0 & 0 & \zeta \end{pmatrix}. \quad (9)$$

Meanwhile the Coulomb interaction term is transformed as:

$$\sum_{\alpha\beta\delta\gamma} U_{\alpha\beta\delta\gamma} d_\alpha^\dagger d_\beta^\dagger d_\delta d_\gamma = \sum_{mnkl} \tilde{U}_{mnkl} c_m^\dagger c_n^\dagger c_k c_l, \qquad (10)$$

with

$$\tilde{U}_{mnkl} = \sum_{\alpha\beta\delta\gamma} U_{\alpha\beta\delta\gamma} \mathcal{A}_{m\alpha}^\dagger \mathcal{A}_{n\beta}^\dagger \mathcal{A}_{\delta k} \mathcal{A}_{\gamma l}. \qquad (11)$$
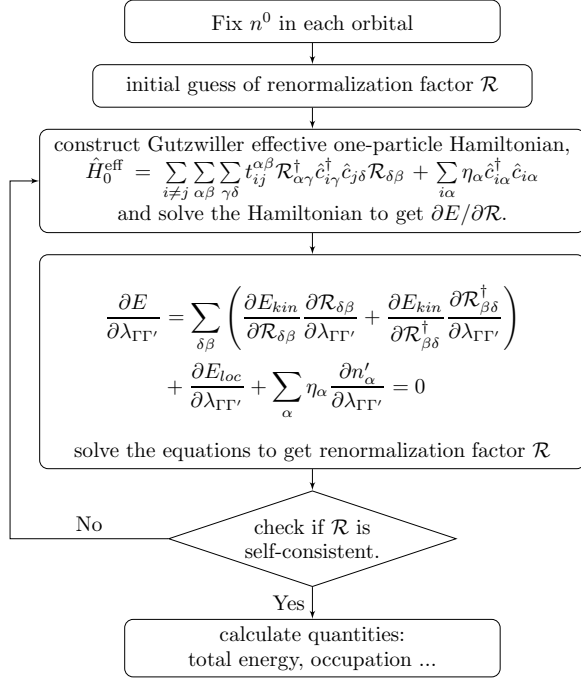

FIG. 1. Flowchart of the RIGA self-consistent loop to minimize total energy $E(n^0)$ with respect to $|\Psi_0\rangle$ and $\lambda_{\Gamma\Gamma'}$.

In this paper, we define expectation value with uncorrelated wave function:

$$O^0 = \langle \Psi_0 | \hat{O} | \Psi_0 \rangle, \qquad (12)$$

while expectation value with Gutzwiller wave function is defined as:

$$O = O^G = \langle \Psi_G | \hat{O} | \Psi_G \rangle. \qquad (13)$$

During the minimization process, two following constraints are forced,

$$\langle \Psi_0 | \mathcal{P}^\dagger \mathcal{P} | \Psi_0 \rangle = 1, \qquad (14)$$

and

$$\langle \Psi_0 | \mathcal{P}^\dagger \mathcal{P} n_{i\alpha} | \Psi_0 \rangle = \langle \Psi_0 | n_{i\alpha} | \Psi_0 \rangle. \qquad (15)$$

In the present paper, the second constraint is satisfied in the following way. We first calculate the total energy of the trial wave function with both the left-hand and

right-hand side of the above equation equaling to some desired occupation number n_α^0. Then we minimize the energy respect to n_α^0 at the last step.

The remaining task is to minimize the variational ground energy $E = E_{kin} + E_{loc}$ with respect to $\lambda_{\Gamma\Gamma'}$ and $|\Psi_0\rangle$, and fulfill the previous two constraints. Here,

$$E_{kin} = \langle \Psi_G | H_{kin} | \Psi_G \rangle = \sum_{ij} \sum_{\gamma\delta} \tilde{t}_{ij}^{\gamma\delta} \langle \Psi_0 | c_{i\gamma}^\dagger c_{j\delta} | \Psi_0 \rangle, \qquad (16)$$

and

$$E_{loc} = \langle \Psi_G | H_{loc} | \Psi_G \rangle = \text{Tr}(\phi^\dagger H_{loc} \phi), \qquad (17)$$

with $\tilde{t}$, $\mathcal{R}$ and ϕ defined as:

$$\tilde{t}_{ij}^{\gamma\delta} = \sum_{\alpha\beta} t_{ij}^{\alpha\beta} \mathcal{R}_{\alpha\gamma}^\dagger \mathcal{R}_{\delta\beta} \qquad (18)$$

$$\mathcal{R}_{\alpha\gamma}^\dagger = \frac{\text{Tr}(\phi^\dagger c_\alpha^\dagger \phi c_\gamma)}{\sqrt{n_\gamma^0(1 - n_\gamma^0)}}, \qquad (19)$$

$$\phi_{II'} = \langle I | \mathcal{P} | I' \rangle \sqrt{\langle \Psi_0 | I' \rangle \langle I' | \Psi_0 \rangle}, \qquad (20)$$

where $|I\rangle$ ($|I'\rangle$) stands for a many-body Fock state and $n_\gamma^0 = \langle \Psi_0 | n_\gamma | \Psi_0 \rangle$.

The flowchart of RIGA method is shown in Fig.1. For fixed n_α^0 in each orbital, minimizing E with respect to $|\Psi_0\rangle$ and $\lambda_{\Gamma\Gamma'}$ can be divided into two steps in each iterative process. Firstly, fix Gutzwiller variational parameters $\lambda_{\Gamma\Gamma'}$ and find optimal uncorrelated wave function by solving effective single particle Hamiltonian,

$$H_0^{\text{eff}} = \sum_{i \neq j} \sum_{\gamma\delta} \tilde{t}_{ij}^{\gamma\delta} c_{i\gamma}^\dagger c_{j\delta} + \sum_{i\alpha} \eta_\alpha c_{i\alpha}^\dagger c_{i\alpha}, \qquad (21)$$

where Lagrange parameters η_α are used to minimize the variational energy fulfilling Gutzwiller constraints. Secondly, we fix the uncorrelated wave function, and optimize the variational energy with respect to Gutzwiller variational parameters $\lambda_{\Gamma\Gamma'}$,

$$\frac{\partial E}{\partial \lambda_{\Gamma\Gamma'}} = \sum_{\delta\beta} \left(\frac{\partial E_{kin}}{\partial \mathcal{R}_{\delta\beta}} \frac{\partial \mathcal{R}_{\delta\beta}}{\partial \lambda_{\Gamma\Gamma'}} + \frac{\partial E_{kin}}{\partial \mathcal{R}_{\beta\delta}^\dagger} \frac{\partial \mathcal{R}_{\beta\delta}^\dagger}{\partial \lambda_{\Gamma\Gamma'}} \right)$$
$$+ \frac{\partial E_{loc}}{\partial \lambda_{\Gamma\Gamma'}} + \sum_\alpha \eta_\alpha \frac{\partial n_\alpha'}{\partial \lambda_{\Gamma\Gamma'}} = 0, \qquad (22)$$

where $n_\alpha' = \langle \Psi_0 | \mathcal{P}^\dagger \mathcal{P} n_\alpha | \Psi_0 \rangle$. In this way, $\lambda_{\Gamma\Gamma'}$ and $|\Psi_0\rangle$ are self-consistently determined.

For the fix n_α^0 algorithm, we need to scan the n_α^0 to get the global ground state of the studied system. In this paper, because SOC will split the t_{2g} orbitals into two fold $j_{\text{eff}} = 1/2$ and four fold $j_{\text{eff}} = 3/2$ states, we can introduce an alternative variable δn^0 to determine n_α^0 for

each orbital. The occupation polarization δn^0 is defined as:

$$\delta n^0 = n_{3/2}^0 - n_{1/2}^0, \qquad (23)$$

in which $n_{3/2}^0$ and $n_{1/2}^0$ stand for the average occupation number of lower ($j_{\text{eff}} = 3/2$) and upper ($j_{\text{eff}} = 1/2$) orbitals respectively. Since total electron number of the system is fixed to be $4n_{3/2}^0 + 2n_{1/2}^0 = 4$, we have $0 \leq \delta n^0 \leq 1$. δn^0 (n^0) corresponding to ground state is denoted by δn_g^0 (n_g^0).

In the present paper, we also use DMFT+CTQMC method to crosscheck our results derived by RIGA. For DMFT+CTQMC method, the system temperature is set to be $T = 0.025$ (corresponding to inverse temperature $\beta = 40$). In each DMFT iteration, typically 4×10^8 QMC samplings have been performed to reach sufficient numerical accuracy[25].

III. RESULTS AND DISCUSSION

A. U-ζ phase diagram

In this subsection, we mainly focus on phase diagram for the three-band model proposed in Eq.(1). The obtained $U - \zeta$ phase diagrams with $J/U = 0.25$ are shown in Fig.2. The upper panel shows the phase diagram calculated by zero temperature RIGA method, while the calculated results by DMFT+CTQMC method at finite temperature is shown in the lower panel. The results obtained by two different methods are consistent with each other quite well except that DMFT+CTQMC can not distinguish between band insulator and Mott insulator, which will be explained later. Apparently, there exists three different phases in $U - \zeta$ plane: metallic state in the lower left corner, band insulator in the lower right region and Mott insulator in the upper right region. The general shape of the phase diagram can be easily understood by considering two limiting cases: (i) For $\zeta = 0$, one has a degenerate three-band Hubbard model populated by 4 electrons per site. The model will undergo an interaction driven Mott transition at critical $U_c/D \sim 11.0$ with each band filled by $4/3$ electrons. (ii) For non-interacting case ($U = 0.0$), the model is exactly soluble. The three bands are degenerate and filled by $4/3$ electrons at $\zeta=0.0$. Finite ζ will split the three degenerate bands into a (lower) $j_{\text{eff}} = 3/2$ quadruplet and (upper) $j_{\text{eff}} = 1/2$ doublet with energy separation being 1.5ζ. Increasing ζ will pump electrons from upper to lower orbitals until the upper bands are completely empty and the system undergoes a metal to band insulator transition, which is expected at $\zeta/D = 1.33$.

In order to clarify the way we determine the metal, band insulator, and Mott insulator phases by RIGA method, in Fig.3 we plot the total energy and quasiparticle weight as a function of δn^0 defined in the previous section , where the SOC strength is fixed at $\zeta/D = 0.7$,
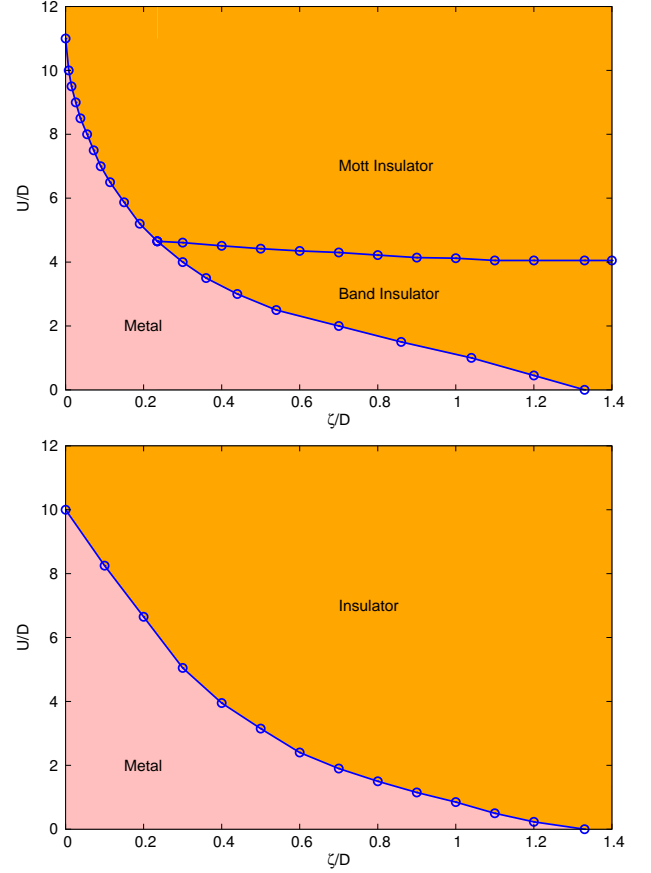

FIG. 2. (Color online) Phase diagram of three-band Hubbard model with full Hund's coupling terms in the plane of Coulomb interaction $U(J/U = 0.25)$ and spin-orbit coupling ζ. Upper panel: The phase diagram is calculated by RIGA at zero temperature. Lower panel: The phase diagram is calculated by DMFT+CTQMC with finite temperature $T = 0.025$.

and from top to bottom the Coulomb interaction is $U/D = 1.0$, 3.0, 6.0. The ground state of the system is the state with the lowest energy respect to δn^0. The typical solution for the metal phase is shown in Fig.3a, where the energy minimum occurs at $0 < \delta n_g^0 < 1.0$ corresponding to the case that all orbitals being partially occupied. While for a band insulator, as shown in Fig.3b as a typical situation, the energy minimum happens at $\delta n_g^0 = 1.0$ corresponding to the case that the $j_{\text{eff}} = 3/2$ orbitals are fully occupied and $j_{\text{eff}} = 1/2$ orbitals are empty, and more over the quasiparticle weight Z keeps finite when δn^0 approching unit. And finally the situation of a Mott insulator is illustrated in Fig.3c, where the quasiparticle weight Z vanishes at some critical δn^0, above which the system is in Mott insulator phase and can no longer be described by the Gutzwiller variational method.

While in the DMFT+CTQMC calculations, the phase boundary between metal and insulator is identified by measuring the imaginary-time Green function at $\tau = \beta/2$[26,27]. Since $G(\beta/2)$ can be viewed as a representa-
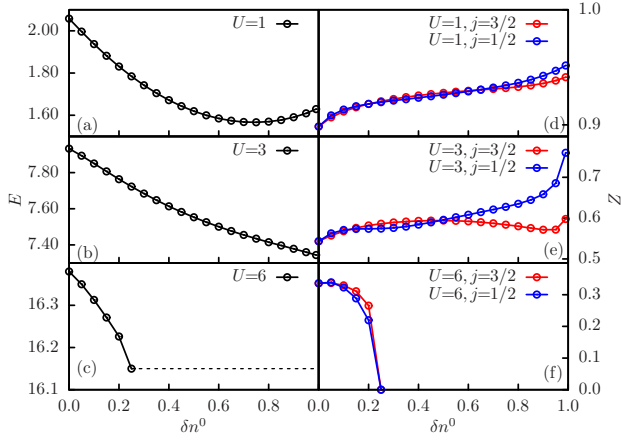
FIG. 3. (Color online) Total energy $E(\delta n^0)$ and quasiparticle weight $Z(\delta n^0)$ as a function of occupation polarization $\delta n^0 = n_{3/2}^0 - n_{1/2}^0$ for different values of interaction strength $U/D = 1,\ 3,\ 6\ (J/U = 0.25)$ at fixed $\zeta/D = 0.7$ and zero temperature, where $n_{3/2}^0$ is average occupation number of $j_{\text{eff}} = 3/2$ quadruplet, $n_{1/2}^0$ is average occupation number of $j_{\text{eff}} = 1/2$ doublet.

FIG. 4. (Color online) The imaginary-time Green function at $\tau = \beta/2$ as a function of Coulomb interaction strength U. The SOC strength ζ is chosen to be 0.5 as a illustration. The calculation is done by DMFT+CTQMC method at $\beta = 40$. In this figure the normalized quantities by $G(\beta/2)$ at $U/D = 1.0$ are shown and the arrows correspond to phase transition points.

tion of the integrated spectral weight within a few $k_B T$ of E_F, so it can be used as an important criterion to judge whether metal-insulator transition occurs. The corresponding results for SOC strength $\zeta/D = 0.5$ are shown in Fig.4. Clearly seen in this figure, the critical U_c is about 3.5, and both the $j_{\text{eff}} = 3/2$ and $j_{\text{eff}} = 1/2$ orbitals undergo metal-insulator transitions simultaneously. Since there is chemical potential ambiguity in the insulator phase, it is difficult to further distinguish Mott insulator from band insulator by DMFT+CTQMC method. Therefore we only calculate the phase boundary between the metal and insulator phase, which is in good agreement with the results obtained by RIGA.

Now, we come back to discussed the phase diagram obtained by RIGA and DMFT. When both the Coulomb interaction U and SOC ζ are finite, the phase diagram looks a bit complicated. By considering different values of SOC, we divide the phase diagram vertically into three regions.

Firstly, for $0.00 < \zeta/D < 0.24$, with increasing Coulomb interaction U, our calculation by RIGA predicts a transition from metal to Mott insulator. The transition is characterized by the vanishing of quasiparticle weight as discussed previously. The critical Coulomb interaction U_c decreases drastically with the increment of SOC, the effect of SOC tends to enhance the Mott MIT greatly. The DMFT results show very similar behavior in this region as shown in lower panel of Fig.2, except that the U_c obtained by DMFT has weaker dependence on the strength of SOC compared to that of RIGA. From the view point of DMFT, the suppression of the metallic phase by SOC can be explained quite clearly. For the effective impurity model in DMFT, the metallic phase corresponds to a solution when the local moments on the
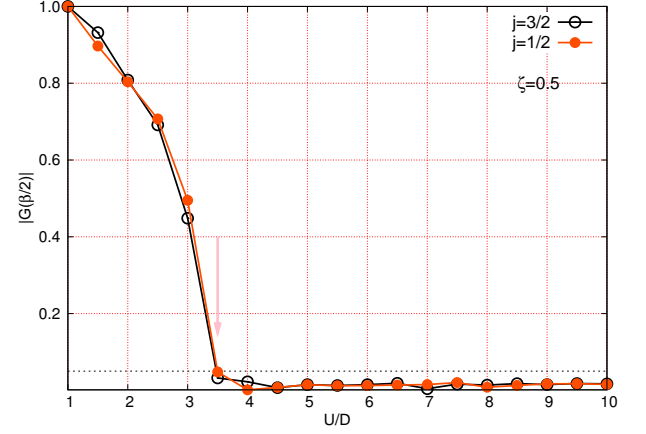
impurity site are fully screened by the electrons in heat-bath through the Kondo like effect. With the SOC, there is an additional channel to screen the local spin moment other than the Kondo effect, which leads to the formation of spin-orbital singlets. This additional screening channel, which is completely local, will thus compete with the Kondo effect and suppress the metallic solution. There is no net local moment left in this type of Mott phase, and the ground state is simply a product state of local spin-orbital singlets on each site.

For $0.24 < \zeta/D < 1.33$, two successive phase transitions are observed with the increment of U. The transition from metallic to band insulator phases occurs firstly, and followed by another transition to the Mott insulator phase. In the intermediate U region, the effective band width of system is reduced by the correlation effects, which drives the system into a band insulator phase with relative small band splitting induced by SOC. Further increasing interaction strength U will push the system to the Mott limit. Although this process is believed to be a crossover rather than a sharp phase transition, our RIGA calculation provides a mean field description for these two different insulators, where in the band insulator phase the interaction effects only renormalize the effective band structure and do not suppress the coherent motion of the electrons entirely. Similar behavior can also be obtained by DMFT method, where the quasiparticle weight determined by DMFT selfenergy keeps finite for the band insulator phase and vanishes for the Mott insulator phase.

At last, for $\zeta/D > 1.33$ region, the orbitals are fully polarized with electrons fully occupied $j_{\text{eff}} = 3/2$ bands and fully empty $j_{eff} = 1/2$ bands at $U = 0.0$, indicating that the system is in the band insulator state already

in the non-interacting case. Similar band insulator to Mott insulator transition will be induced with further increment of U in the RIGA description, as discussed before.
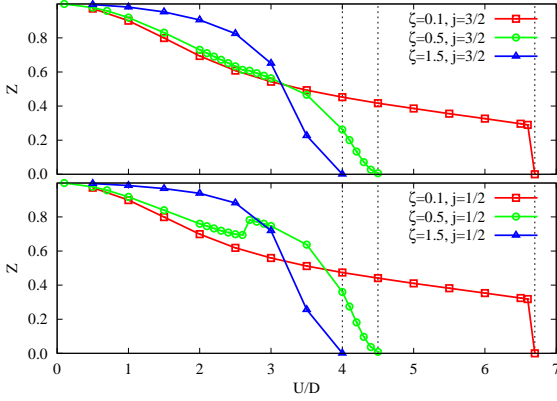

FIG. 5. (Color online) Quasiparticle renormalization factors Z of the lower orbitals ($j_{\text{eff}} = 3/2$ quadruplet) and upper orbitals ($j_{\text{eff}} = 1/2$ doublet) as function of Coulomb interaction $U(J/U = 0.25)$ for different values of SOC ($\zeta/D = 0.1, 0.5, 1.5$). The dashed lines label the critical U for transition to Mott state. The results are obtained by zero temperature RIGA method.
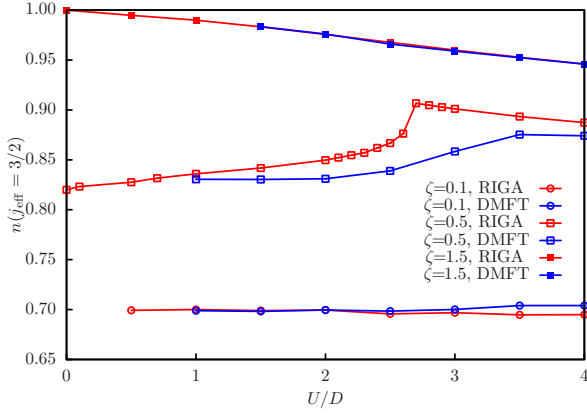
FIG. 6. (Color online) Occupation number of the lower orbitals ($j_{\text{eff}} = 3/2$ quadruplet) with increasing Coulomb $U(J/U = 0.25)$ for selected SOC ($\zeta/D = 0.1, 0.5, 1.5$). Both the calculated results by RIGA and DMFT(CTQMC) are presented.

For several typical SOC parameters ($\zeta/D = 0.1, 0.5, 1.5$) in the three regions defined above, we study the evolutions of quasiparticle weight and band specific occupancy with Coulomb interaction. The quasiparticle weight for selected SOC with increasing U is plotted in Fig.5. The upper (lower) panel shows the quasiparticle weight for $j_{\text{eff}} = 3/2$ (1/2) orbitals. Note the quasiparticle weight in RIGA is defined as the eigenvalues of the Hermite matrix $\mathcal{R}^{\dagger}\mathcal{R}$. For both $\zeta/D = 0.1$ and 1.5,
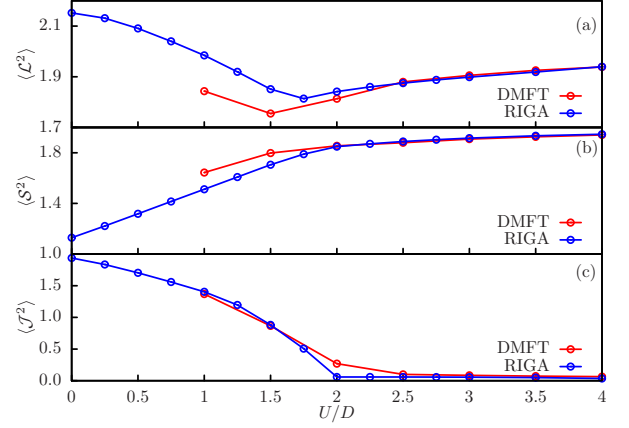

FIG. 7. (Color online) Expectation value of orbital angular momentum $\langle \mathcal{L}^2 \rangle$, spin angular momentum $\langle \mathcal{S}^2 \rangle$, and total angular momentum $\langle \mathcal{J}^2 \rangle$ as function of Coulomb interaction U with fixed spin-orbit coupling strength $\zeta/D = 0.7$. It is derived by RIGA at zero temperature and DMFT+CTQMC at $\beta = 40$ respectively.

the quasiparticle weights decrease from 1 to 0 monotonically with the increasing interaction strength U and J until the transition to Mott insulator phase. While for $\zeta/D = 0.5$, there exists a kink at $U/D = 2.7$ in the lower panel ($j_{\text{eff}} = 1/2$), which corresponds to the transition from metal to band insulating state. For transition to Mott insulating state, quasiparticle weights for all the orbitals reach zero simultaneously, with $U_c/D = 6.7$ for $\zeta/D = 0.1$, $U_c/D = 4.5$ for $\zeta/D = 0.5$, and $U_c/D = 4.0$ for $\zeta/D = 1.5$.

The occupation number of the (lower) $j_{\text{eff}} = 3/2$ orbitals as a function of on-site Coulomb interaction U is ploted in Fig.6 for three typical SOC strength. For $\zeta/D = 0.1$, to some extent, the occupation behavior is similar to $\zeta = 0$ case, in which the occupation number is only slightly changed by the interaction. The situation is quite different for $\zeta/D = 0.5$, where the occupation of the $j_{\text{eff}} = 3/2$ orbital increases with interaction at the beginning and decreases slightly after the transition to the band insulator phase. The non-monotonic behavior here is mainly due to the competition between the repulsive interaction U and Hund's rule coupling J. The effect of U will always enhance the splitting of the local orbitals to reduce the repulsive interaction among these orbitals. While the Hund's rule coupling intents to distribute the electrons more evenly among different orbitals. For $\zeta/D = 1.5$ case, occupation number in the two subsets is fully polarized at $U = 0$ and the effect of Hund's coupling term will reduce the occupation of the $j_{\text{eff}} = 3/2$ orbital monotonically.

At last, the expectation value of the total orbital angular momentum $\langle \mathcal{L}^2 \rangle$, spin angular momentum $\langle \mathcal{S}^2 \rangle$ and total angular momentum $\langle \mathcal{J}^2 \rangle$ as a function of Coulomb interaction U are plotted in Fig.7, where ζ/D is fixed to 0.70. In the non-interacting case, all the three ex-

pectation values can be calculated exactly and they will approach the atomic limit with the increment of interaction U and J. In the atomic limit the SOC strength is much weaker than the Hund's coupling J, the ground state can be well described by the LS coupling scheme, where the four electrons will first form a state with total orbital angular momentum $\mathcal{L} = 1$ and total spin momentum $\mathcal{S} = 1$, and then form a spin-orbital singlet state with total angular momentum $\mathcal{J} = 0$. From Fig.7, we can find that the system approaches the spin-orbital singlet quite rapidly after the transition to the band insulator phase.
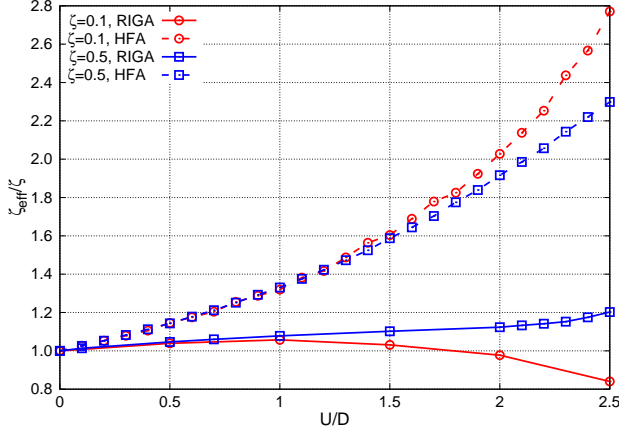

FIG. 8. (Color online) Evolution of effective SOC strength with increasing Coulomb $U(J/U = 0.25)$ for selected SOC $(\zeta/D = 0.1, 0.5)$, A comparison of results derived by RIGA and HFA are presented.

B. Effective spin-orbit coupling

In the multi-orbital system, the interaction effects will mainly cause two consequences for the metallic phases: (1) It will introduce renormalization factor for the energy bands; (2) It will modify the local energy level for each orbital which splits the bands. For the present model, the second effect will modify the effective SOC, which is another very important problem for the spin orbital coupled correlation system. Within the Gutzwiller variational scheme used in the present paper, the effective SOC can be defined as:

$$\zeta_{\text{eff}} = -\frac{1}{2}\frac{\partial E_{int}(\delta n^0)}{\partial \delta n^0} - \frac{1}{2}\frac{\partial E_{soc}(\delta n^0)}{\partial \delta n^0}, \qquad (24)$$

where E_{int} and E_{soc} are the ground state expectation values of interaction and SOC terms in the Hamiltonian respectively. Note the second term is different from the bare SOC ζ_0 unless n_α is a good quantum number. If the interaction energy is treated by Hartree Fock mean field approximation (HFA), the above equation gives $\zeta_{\text{eff}} = -\partial E_{int}^{HF}(\delta n^0)/(2\partial \delta n^0) + \zeta_0$, which will always greatly enhance the spin-orbital splitting with the increasing U as found by some works based on LDA+U

method[28,29]. In this section, we compare the results obtained by RIGA and HFA. As shown in Fig.8, the effective SOC obtained by HFA increases quite rapidly with the interaction U and J. While the results obtained by RIGA show very different behavior. For weak SOC strength, i.e. $\zeta/D = 0.1$, the effective SOC obtained by RIGA increases first then decrease. This interesting non-monotonic behavior reflects the competition between the repulsive interaction U, which intends to increase the occupation difference for $j_{\text{eff}} = 1/2$ and $j_{\text{eff}} = 3/2$ orbitals, and the Hund's rule coupling J, which intents to decrease the occupation difference. While for relatively strong SOC strength, the effective SOC increases with interaction U (and J) monotonically all the way to the phase boundary indicating the repulsive interaction U plays a dominate role here. But compared to HFA, the enhancement of effective SOC induced by the interaction is much weaker even for the latter case. This is mainly due to the reduction of the high energy local configurations in the Gutzwiller variational wave function compared to the Hatree Fock wave function, which greatly reduces the interaction energy and its derivative to the orbital occupation.

IV. CONCLUDING REMARKS

The Mott MIT in three-band Hubbard model with full Hund's rule coupling and SOC is studied in detail using RIGA and DMFT+CTQMC methods. First, we propose the phase diagram with the strength of electron-electron interaction and SOC. Three different phases have been found in the $U - \zeta$ plane, which are metal, band insulator and Mott insulator phases. For $0.00 < \zeta/D < 0.24$, increasing Coulomb interaction will induce a MIT transition from metal to Mott insulator. For $0.24 < \zeta/D < 1.33$, effect of U will cause two successive transitions, first from metal to band insulator, then to Mott insulator. For $\zeta/D > 1.33$, a transition from band insulator to Mott insulator is observed. From the phase diagram, we find that the critical interaction strength U_c is strongly reduced by the presence of SOC, which leads to the conclusion that the SOC will greatly enhance the strong correlation effects in these systems. Secondly, we have studied the effect of electron-electron interaction on the effective SOC. Our conclusion is that the enhancement of effective SOC found in HFA is strongly suppressed once we go beyond the mean field approximation and include the fluctuation effects by RIGA or DMFT methods.

ACKNOWLEDGMENT

[1] M. Imada, A. Fujimori, and Y. Tokura, Rev. Mod. Phys. **70**, 1039 (1998).

[2] A. Georges, G. Kotliar, W. Krauth, and M. J. Rozenberg, Rev. Mod. Phys. **68**, 13 (1996).

[3] G. Kotliar, S. Y. Savrasov, K. Haule, V. S. Oudovenko, O. Parcollet, and C. A. Marianetti, Rev. Mod. Phys. **78**, 865 (2006).

[4] L. de' Medici, J. Mravlje, and A. Georges, Phys. Rev. Lett. **107**, 256401 (2011).

[5] L. de' Medici, S. R. Hassan, M. Capone, and X. Dai, Phys. Rev. Lett. **102**, 126401 (2009).

[6] P. Werner and A. J. Millis, Phys. Rev. Lett. **99**, 126405 (2007).

[7] T. Kita, T. Ohashi, and N. Kawakami, Phys. Rev. B **84**, 195130 (2011).

[8] B. J. Kim, H. Jin, S. J. Moon, J. Y. Kim, B. G. Park, C. S. Leem, J. Yu, T. W. Noh, C. Kim, S. J. Oh, J. H. Park, V. Durairaj, G. Cao, and E. Rotenberg, Phys. Rev. Lett. **101**, 076402 (2008).

[9] D. Pesin and L. Balents, Nature Physics **6**, 376 (2010).

[10] B. J. Kim, H. Ohsumi, T. Komesu, S. Sakai, T. Morita, H. Takagi, and T. Arima, Science **323**, 1329 (2009).

[11] H. Watanabe, T. Shirakawa, and S. Yunoki, Phys. Rev. Lett. **105**, 216410 (2010).

[12] G. Jackeli and G. Khaliullin, Phys. Rev. Lett. **102**, 017205 (2009).

[13] M. Bremholm, S. Dutton, P. Stephens, and R. Cava, Journal of Solid State Chemistry **184**, 601 (2011).

[14] J. Bünemann, W. Weber, and F. Gebhard, Phys. Rev. B **57**, 6896 (1998).

[15] J. Bünemann, F. Gebhard, T. Ohm, S. Weiser, and W. Weber, Phys. Rev. Lett. **101**, 236404 (2008).

[16] N. Lanatà, H. U. R. Strand, X. Dai, and B. Hellsing, Phys. Rev. B **85**, 035133 (2012).

[17] X. Deng, L. Wang, X. Dai, and Z. Fang, Phys. Rev. B **79**, 075114 (2009).

[18] P. Werner and A. Millis, Phys. Rev. B **74**, 1 (2006).

[19] E. Gull, A. J. Millis, A. I. Lichtenstein, A. N. Rubtsov, M. Troyer, and P. Werner, Rev. Mod. Phys. **83**, 349 (2011).

[20] W. Metzner and D. Vollhardt, Phys. Rev. Lett. **59**, 121 (1987).

[21] W. Metzner and D. Vollhardt, Phys. Rev. B **37**, 7382 (1988).

[22] M. C. Gutzwiller, Phys. Rev. Lett. **10**, 159 (1963).

[23] M. C. Gutzwiller, Phys. Rev. **134**, A923 (1964).

[24] M. C. Gutzwiller, Phys. Rev. **137**, A1726 (1965).

[25] L. Huang, L. Du, and X. Dai, Phys. Rev. B **86**, 035150 (2012).

[26] A. Liebsch, Phys. Rev. Lett. **91**, 226401 (2003).

[27] L. Huang, Y. Wang, and X. Dai, Phys. Rev. B **85**, 245110 (2012).

[28] G.-Q. Liu, V. N. Antonov, O. Jepsen, and O. K. Andersen., Phys. Rev. Lett. **101**, 026408 (2008).

[29] A. Subedi, Phys. Rev. B **85**, 020408 (2012).